Appl. Phys. B 78, 241–248 (2004)
DOI: 10.1007/s00340-003-1362-9

Applied Physics B
Lasers and Optics

H. BLADH✉
P.-E. BENGTSSON

Characteristics of laser-induced incandescence from soot in studies of a time-dependent heat- and mass-transfer model

Department of Combustion Physics, Lund Institute of Technology, P.O. Box 118, 22100 Lund, Sweden

Received: 25 April 2003/Revised version: 8 October 2003
Published online: 19 December 2003 •

ABSTRACT The temporal behavior of the laser-induced incandescence (LII) signal is often used for soot-particle sizing, which is possible because the cooling behavior of a laser-heated particle is dependent on the particle size. The heat- and mass-transfer model describing the temporal LII-signal behavior has in this work been extended to include the influence of the primary particle-size distribution and the spatial distribution of laser energy. When evaluating primary particle size, a monodisperse size distribution is often assumed, although it is well known that a polydisperse distribution is a better description of the real situation. In this work the impact of this assumption is investigated for Gaussian and lognormal size distributions of different widths, and the result is a significant bias towards larger particle sizes because of the higher influence of larger particles on the LII signal. Moreover, the dependence of the LII signal on the laser fluence is studied for different spatial distributions of the laser energy. The top-hat, Gaussian sheet and Gaussian beam distributions were tested and it is established that the LII signal is strongly dependent on the choice of distribution. However, in this case the influence of particle size is minor.

PACS 02.30.Hq; 44.40.+a

1 Introduction

Quantitative measurements of soot properties are of great importance in the quest of reducing particle emissions from combustion processes. Soot is formed in locally fuel-rich zones at elevated temperatures, a situation that for instance occurs in Diesel engines, and the presence of soot can be seen as an indicator of an insufficient combustion process. Soot particles are also unhealthy for humans since they are small enough to follow the breathing air into the lungs where they can be deposited, and polyaromatic hydrocarbons (PAHs) condensed on the soot surface increase the risk of cancer [1]. There is an increasing need for powerful tools that are able to quantify the amount of soot as well as its properties. Laser-induced incandescence (LII) has proved to be a promising technique in this respect. The technique is based on measurements of the Planck radiation from laser-heated soot particles and, dependent on the choice of detector and data analysis, the technique may yield both the soot volume fraction and the soot primary particle size.

Measurements of the soot volume fraction have turned out to be relatively straightforward since this quantity, as shown by Melton [2] and later also others (see for example [3] and references herein), is approximately proportional to the LII signal in the visible-wavelength region. For quantitative data of the soot volume fraction the signal must be calibrated. Several approaches have been developed and the most common is to measure light extinction in a flat calibration flame (see for example Bengtsson and Aldén [4]). This technique has also been successfully applied in an online setup [5]. The sensitivity of this technique can be further enhanced by using a cavity ringdown setup [6, 7].

For particle-size measurements the time-resolved signal has been studied, since the decay of the signal reflects the particle cooling, which in turn is dependent on the particle size [2, 8–11]. The technique is then often referred to as time-resolved laser-induced incandescence (TIRE-LII). The interpretation of the results is here much more complicated than for the soot volume fraction. Attempts have been made to calibrate primary particle sizes by using flames in which the particle sizes are measured using thermophoretic sampling and transmission electron microscopy (TEM) [12]. Even if this approach is possible, it is complicated and time consuming. Therefore, one usually uses a theoretical model of the time-resolved LII signal for evaluation of the primary particle size.

The time-resolved LII signal is derived from a heat- and mass-transfer model for soot particles that are heated by laser radiation. Models used today are based on the one presented by Melton in 1984 [2], where the basic principle is heat- and mass-balance equations for a single spherical soot particle exposed to an intense laser pulse. Since Melton's work, different improvements of the model have been made and which is the best choice can be argued. Roth and Filippov developed a model which had the benefit of yielding an analytical expression for the decay constant [11]. However, their model does not treat soot vaporization and can thus not be utilized at high laser fluences. Usually the vaporization process is included in the model. The process is treated as a surface vaporization and the primary particle size is thus a function of time. Smallwood et al. discussed the treatment of soot vaporization in the model [13]. The heat transfer from the heated particle to the

✉ Fax: +46-46/222-45-42, E-mail: henrik.bladh@forbrf.lth.se

surrounding gas is another area for which different treatments are found. One of the reasons is that a typical LII application makes it necessary to use an expression valid for the transition regime between the free-molecular and the continuum regime [14, 15].

Recently, a thorough investigation of the physical processes involved during the soot-particle heating process has been performed by Michelsen [16]. Attempts have been made to model not only heating and cooling of the particles, but also structural changes due to the intense laser radiation. It is proposed that processes like Stephan flow (transport of mass and energy away from a particle undergoing vaporization, thus reducing the heat-transfer rate) and thermal annealing (structural changes within the soot particles because of the high temperature when exposed to the laser pulse) may be important. This new model has been used for comparison with detailed measurements by Witze et al. [17], and some improvement in comparison with previous models could be observed [16].

Previous studies of TIRE-LII have identified a number of uncertainties in the evaluation of the signal in terms of particle size. The temperature of the surrounding gas must be known for the heat-transfer term to predict the cooling rate properly, and Will et al. have shown that the error in evaluated particle size introduced by an uncertainty in gas temperature is quite large [10]. Much of the optical data for soot that is needed for the model to be able to yield proper predictions is unknown. Usually data for carbon is used. The hydrogen content of soot may differ substantially at different regions in flames and for different flames, which may give varying material properties that affect the primary particle size. Other implications are that soot primary particles in real combustion processes form clusters, and in addition they have a size distribution. Also, the spatial energy distribution of the exciting laser pulse has a great impact on the overall signal, since the particles are exposed to different laser fluences.

In the present study we have concentrated on two parameters only and their influence on the TIRE-LII signals: the primary particle-size distribution and the spatial laser-energy distribution. The previous TIRE-LII model has therefore been extended to be able to accommodate these parameters. The model has been used to predict the fluence dependence of the integrated TIRE-LII signal for different spatial distributions of laser energy. We also present predictions of the overestimation introduced in the evaluated primary particle size when assuming monodisperse particle-size distributions when the real distribution is polydisperse.

2 Theory

Although the attempts at developing a model for TIRE-LII have used the same basic principles, the point has not been reached where the researchers on LII use the same formulas and parameters for the evaluation. The current work is based on the treatment presented by Snelling et al. [18] and Smallwood et al. [13], a treatment that is much related to that of Hofeldt [9]. The two balance equations can be written according to (1).

$$\begin{aligned}&\frac{\pi^2 D^3 E(m)}{\lambda} q(t) - \frac{2k_\mathrm{a}(T-T_\mathrm{g})\pi D^2}{D + G\lambda_\mathrm{MFP}} + \frac{\Delta H_\mathrm{v}}{M_\mathrm{v}} \frac{\mathrm{d}M}{\mathrm{d}t} \\ &+ q_\mathrm{rad} - \frac{1}{6}\pi D^3 \varrho_\mathrm{s} c_\mathrm{s} \frac{\mathrm{d}T}{\mathrm{d}t} = 0, \\ &\frac{\mathrm{d}M}{\mathrm{d}t} = \frac{1}{2}\varrho_\mathrm{s}\pi D^2 \frac{\mathrm{d}D}{\mathrm{d}t} = -\pi D^2 \beta P_\mathrm{v}(T)\sqrt{\frac{M_\mathrm{v}}{2\pi RT}}.\end{aligned} \tag{1}$$

The parameters are given in Table 1 and Fig. 1. For the refractive index, m, the value from Dalzell and Sarofim has been used [19]. Some properties of soot are unknown, and in these cases data of carbon has been used instead [20]. The other parameters have been chosen from Smallwood et al. [13]. From (1) a pair of coupled first-order differential equations can be

Notation	Parameter	Values used	Unit	Reference
D	Primary particle diameter	Variable	m	
$E(m)$	Refractive index function for absorption	$\mathrm{Im}((m^2-1)/(m^2+2))$	-	
λ	Laser wavelength	532×10^{-9}	m	
$q(t)$	Laser irradiance	Gaussian, 10 ns FWHM	$\mathrm{W/m^2}$	
k_a	Heat conduction coefficient of air	0.12	W/mK	[13]
T	Particle temperature	Variable	K	
T_g	Temperature of surrounding gas	1800	K	
G	Geometry-dependent heat transfer factor	22.064	-	[13]
λ_MFP	Mean free path	0.5665×10^{-6}	m	[13]
ΔH_v	Heat of vaporization of soot	See Fig. 1	J/mole	[13]
M_v	Molecular weight of soot vapor	See Fig. 1	kg/mole	[13]
R	Universal gas constant	8.31	J/moleK	
β	Evaporation coefficient	0.8	-	[18]
ϱ_s	Density of soot	2.2×10^{-3}	$\mathrm{kg/m^3}$	[13]
c_s	Specific heat of soot	2.1×10^{-3}	J/kgK	[13]
k	Boltzmann's constant	1.38×10^{-23}	J/K	
h	Planck's constant	6.63×10^{-34}	Js	
c	Velocity of light	2.997×10^{8}	m/s	
P_v	Vapor pressure of soot	See Fig. 1	Pa	[13]
m	Refractive index of soot	1.56–0.46i	-	[19]
$R(\lambda)$	Spectral response function	Not used	-	
ε	Emission coefficient	$4\pi D\cdot E(m)/\lambda$	-	[18]
M^b_λ	Blackbody spectral radiation function	See for instance [10, 18]	$\mathrm{W/m^3}$	-

TABLE 1 The parameters and functions in the heat- and mass-transfer model for TIRE-LII. Many of these parameters have not been altered since they have not been the focus of this study

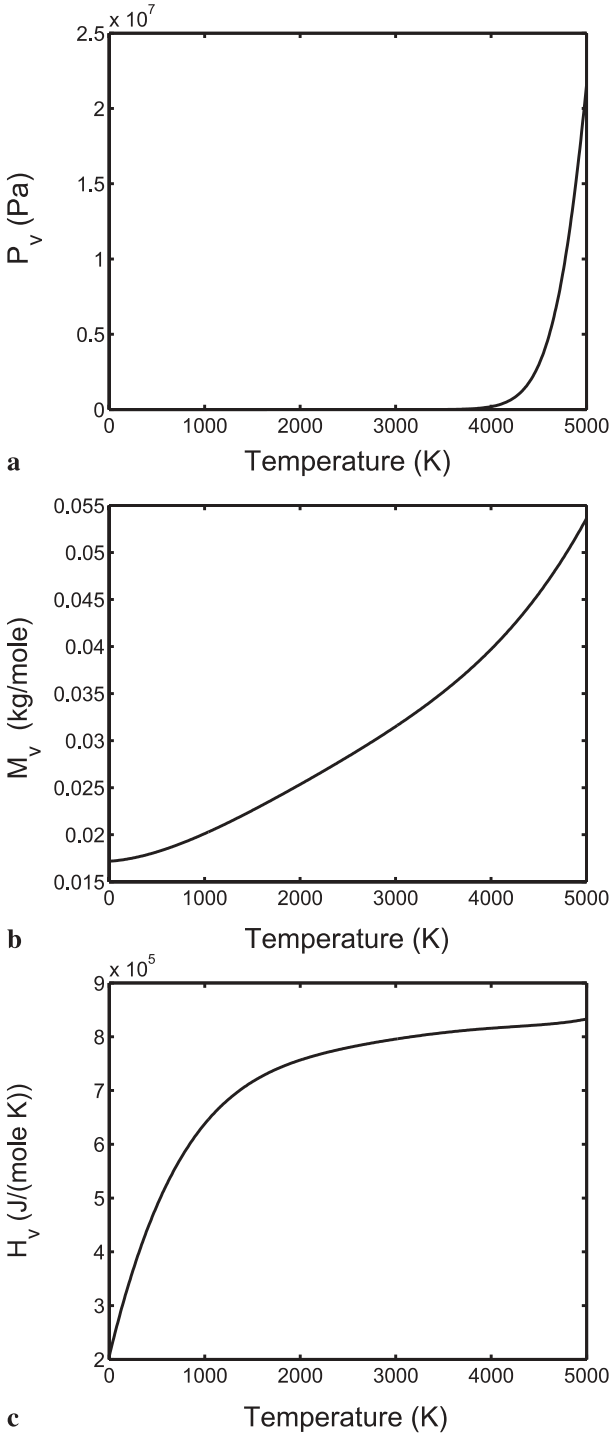

FIGURE 1 The vapor pressure, molecular weight and heat of vaporization of carbon as a function of temperature. These functions have been used in the present study as values for soot, and they have been derived using data from Smallwood et al. [13] originally derived from thermodynamic calculations by Leider et al. [20]

formed and these are solved numerically for the unknown functions $T(t)$ and $D(t)$. The signal is calculated using these functions and the general expression has been given by Will et al. as the expression in (2) [10].

$$S_{\mathrm{LII}} \propto D^2 \int R(\lambda)\varepsilon(D,\lambda)M_\lambda^b(T,\lambda)\,\mathrm{d}\lambda. \qquad (2)$$

However, in the present study the signal is derived using single-wavelength detection, thus avoiding this numerical integration routine. In addition, the term q_{rad}, which also has to be integrated over wavelengths, is set to zero, since it has been shown to be orders of magnitude smaller than the other terms [10, 18]. These two simplifications make the computational time much less since two numerical integration routines can be avoided. No detailed studies dealing with parameters and terms in these equations will be presented here.

3 Extension of the heat- and mass-transfer model

Equations (1) are derived for a single spherical particle of a certain size exposed to a certain laser energy. This means that the equations in a real situation should be applicable only to soot with a monodisperse size distribution where the particles are exposed to equal fluence ($\mathrm{J/cm^2}$), for example a top-hat spatial distribution of the laser energy (Fig. 2a). Usually the laser energy has a non-uniform spatial distribution. Ideally it is Gaussian. Here different cases occur dependent on the beam-shaping optics. For imaging measurements a laser sheet is usually formed using cylindrical optics. If only the central region of the sheet is used for the measurements this would yield a top-hat–Gaussian distribution, here called a Gaussian sheet (see Fig. 2b). For point measurements the beam is focused with a spherical lens which, without any apertures, yields a circular symmetric Gaussian distribution, here called a Gaussian beam (Fig. 2c).

The primary particles have a certain size distribution, which generally is assumed to be somewhat skewed, and is therefore often fitted to lognormal distributions [21]. Sometimes a Gaussian distribution has been considered to describe the real distribution adequately [22].

The extension of the model to include size and spatial energy distributions uses the method of linear combination, where the system of (1) and the LII signal response, (2), is solved for a discrete number of values of the initial diameter D^0 and the laser fluence F. The chosen diameter D^0 is given for the differential equation solver as an initial value for $D(t)$, whereas the fluence F is used by the program to derive the time-dependent laser irradiance function $q(t)$ according to

$$q(t) = F \times f(t), \qquad (3)$$

where $f(t)$ is the temporal distribution function for the laser-pulse energy. If not specified otherwise, the temporal distribution is Gaussian with a duration of 10 ns using the full width at half maximum (FWHM). The resulting TIRE-LII-signal curves from the numerous calculations are later added in fractions determined by the distribution functions for D^0 and F. The method follows four main steps as depicted in Fig. 3.

In step 1 the distribution functions are used to determine the set of different values of the parameters D^0 and F. The program performs calculations for any parameter for which the distribution function exceeds 1% of its maximum value. In step 2 (1) are solved for all combinations of the determined values. In step 3 the TIRE-LII signal is derived using (2) and in step 4 the distribution functions are used to derive the coefficients in the linear combination. For the spatial distributions, the coefficients are determined by the amount of soot exposed to a certain energy. For the Gaussian sheet

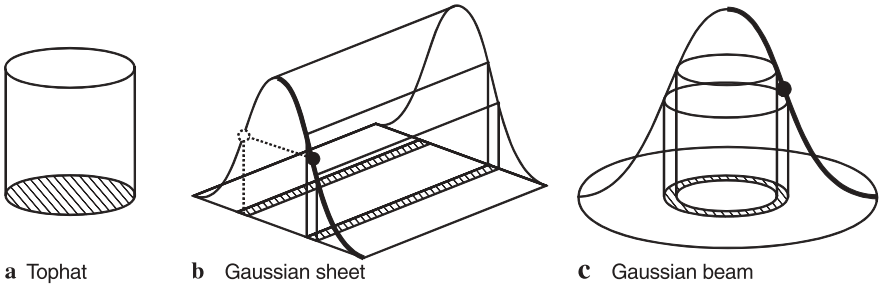

FIGURE 2 3D view of the three different spatial distributions of laser energy used in this study. **a** Uniform laser energy distribution (tophat), **b** Gaussian sheet where one dimension is Gaussian, and **c** Gaussian beam, which is a circular-symmetric Gaussian. The *thick lines* indicate the function along which a discrete number of LII signals are solved. The *marked areas* are used by the linear combination routine to determine the fractions that a certain TIRE-LII-signal curve should add to the overall signal curve

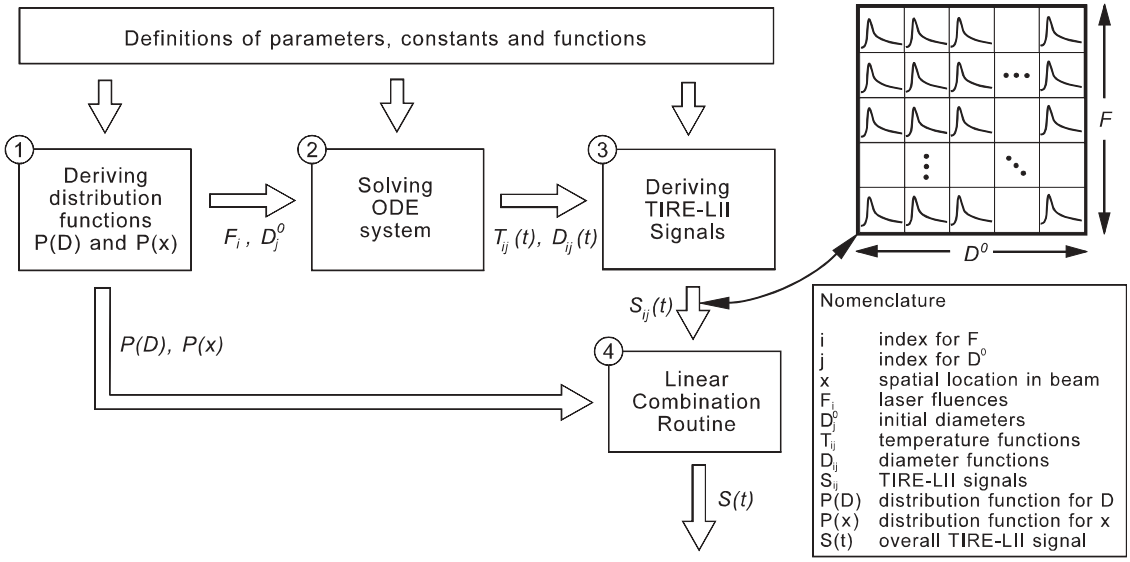

FIGURE 3 A schematic overview of the extended model for TIRE-LII

this is proportional to the rectangular areas in Fig. 2b, and for the Gaussian beam it is proportional to the ring-shaped areas shown in Fig. 2c. It was verified that a resolution of 60 different fluences covering the range of the spatial distributions and 60 different diameters covering the range of the particle-size distributions was satisfactory. This was established by starting at a lower resolution and increasing the number of iterations until the resulting signal curve did not change. It may be noted here that the high resolution is most important for the spatial laser-energy distribution, since the TIRE-LII signal is highly dependent on the laser-energy distribution, whereas it shows less dependence on the particle-size distribution.

4 The monodisperse particle-size approximation

When evaluating data from TIRE-LII measurements, a monodisperse particle-size distribution is often anticipated. In reality the soot particles have a polydisperse size distribution [21, 22]. Since larger particles yield stronger LII signals than smaller, there should be a bias in the evaluation towards larger particles. This is depicted in Fig. 4.

Generally, the real distribution is considered narrow enough not to affect the results to a large extent. However, to the authors' knowledge, no thorough investigation has been presented where the bias has been quantified. Using the extended TIRE-LII model for polydisperse primary particle-size distributions with a certain average particle diameter and comparing the resulting signal decay with monodisperse signal decays, a best fit can be found for a certain

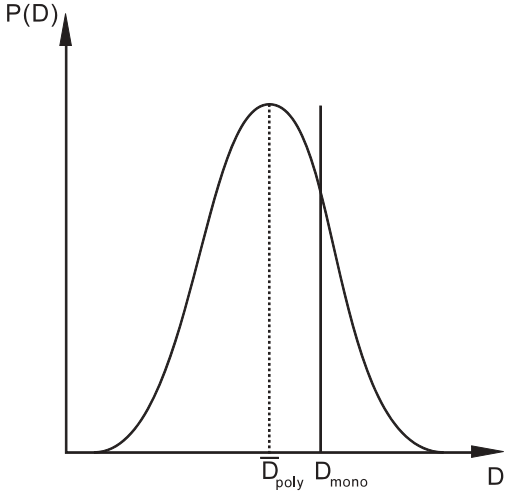

FIGURE 4 When the LII-signal decay is used for evaluating the primary particle size using a model that works with monodisperse distributions, a bias is introduced yielding a primary particle size (D_{mono}) larger than the mean of the distribution ($\bar{D}_{poly}$). The figure illustrates the effect for a Gaussian soot particle size distribution

monodisperse particle diameter. When comparing with the polydisperse distribution, a parameter has to be chosen. For the Gaussian distribution this naturally becomes the mean of the distribution.

A peak fluence just below the vaporization threshold was chosen in these calculations to avoid any impact of vaporization, since this process initiates particle-size reduction, thus

making interpretation of data more complicated. The TIRE-LII signals were calculated for a 600-ns interval, and were normalized at a time after the prompt signal where other effects than the heat transfer were considered negligible. The best fit was found by calculating the variance between the values in the polydisperse decay and the values in different monodisperse decays, finding the minimum of these variances. The method was used iteratively. The curve shapes of the TIRE-LII signal derived from the polydisperse and monodisperse distributions are not exactly equal. However, the differences are so small that they are considered negligible compared to the uncertainty introduced in an experiment using for instance a PMT. The interpreted monodisperse primary particle size for a Gaussian size distribution is given in Fig. 5. All calculations are performed with a top-hat spatial laser-energy distribution.

It is shown in Fig. 5 that, for a FWHM 60% of the average diameter, the bias approaches 8 nm for the 50-nm particle. The question is if these distributions are representative for real soot. Köylü and Faeth determined that the standard deviations of their measured primary particle-size distributions were in the range 17%–25% of the mean primary particle diameter [22]. In FWHM of a Gaussian distribution this would mean 40%–60%, which shows that our results are highly relevant for a real measurement situation.

As previously mentioned, measured particle-size distributions have often been fitted with a lognormal distribution [21, 23]. Therefore, lognormal distributions were tested and the biases compared to the ones introduced using the Gaussian distribution. For a comparison to be possible the distributions had to be chosen in a certain way. A decision was made to use distributions that have the same average and standard deviation. This makes the lognormal distribution have its peak at shorter diameters than the Gaussian, since the lognormal distribution is skewed. This is illustrated in Fig. 6.

The lognormal and Gaussian distributions generally gave similar biases for the same average and standard deviation of the distributions. However, the lognormal distribution gave somewhat larger biases than the Gaussian and the largest difference occurred for the 60% FWHM Gaussian with average diameter 50 nm. The lognormal distribution gave the bias 10 nm instead of 8 nm for the Gaussian.

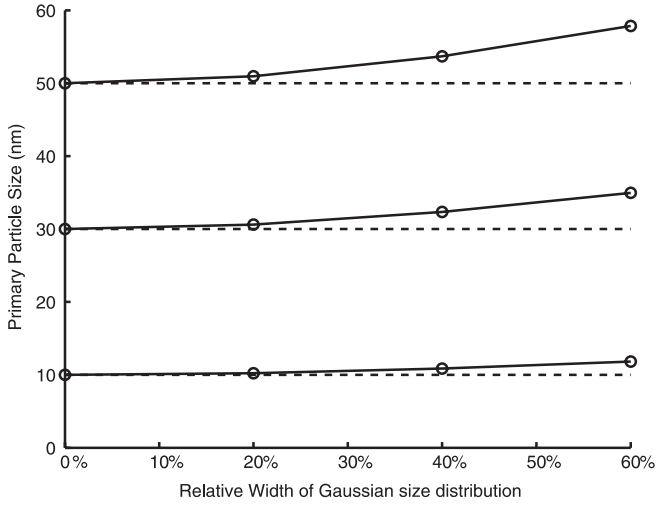

FIGURE 5 The effect of overestimating the primary particle size because of the assumption that the particle-size distribution is monodisperse. The curves show the evaluated monodisperse primary particle size from Gaussian size distributions of different relative widths, where the average size of the distribution is 10, 30 and 50 nm, respectively

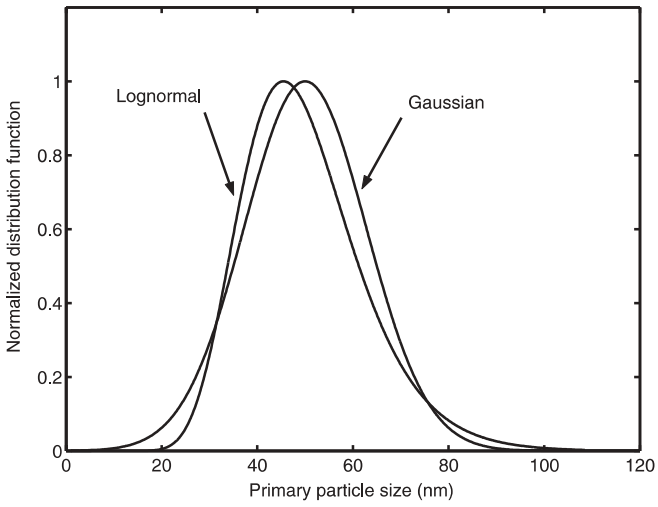

FIGURE 6 The lognormal and Gaussian distributions with equal mean and standard deviation. In this case the mean was 50 nm and the standard deviation 12.7 corresponding to the 60% relative FWHM of the Gaussian function

5 The spatial distribution of laser energy

One of the more well-known properties of LII is the plateau region that often occurs in a plot of LII signal versus laser fluence (here called the fluence curve). This feature of LII is popular among experimentalists, since it enables measurements of LII-signal intensity to be relatively unaffected by fluctuations in the laser-pulse energy. Generally, this behavior is explained by the non-uniform spatial distribution of laser energy, which induces signal contributions from vaporized soot and non-vaporized soot at the same time.

Soot particles that are exposed to a very high fluence will rise to a temperature high enough for vaporization to occur. This makes the LII signal decay faster than it would have without shrinkage, thus making a time-integrated signal covering the decay less than without vaporization. This is illustrated in Fig. 7, where the behavior of the time-resolved LII signal is visualized for a range of fluences. Measurements using different spatial distributions of laser energy have been performed earlier [24, 25], and so have some modeling results [18]. However, these have not been in detail for different shapes of Gaussian distributions and different particle sizes, and a more complete investigation concerning this behavior is here presented.

With the extended model used here, the LII signal as a function of fluence has been calculated for the three spatial distributions of laser energy in Fig. 2. When performing investigations such as this, it is extremely important to be aware of the definitions. The top-hat distribution has finite edges and a constant fluence, while the other two distributions do not. Fluence curves are often presented as a function of mean fluence, i.e. the total pulse energy divided by a certain area, most often using the $1/e^2$ definition for the Gaussian distribution.

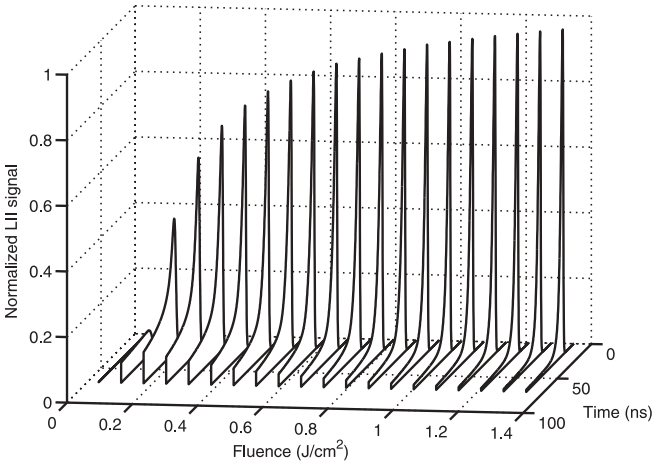

FIGURE 7 The TIRE-LII signal as function of both time and peak fluence for a top-hat profile and primary particle size 50 nm. The signals have been normalized for the peak value of the strongest signal curve. Notice how the maximum of the prompt signal levels out with increasing fluence, while the delayed signal decreases drastically

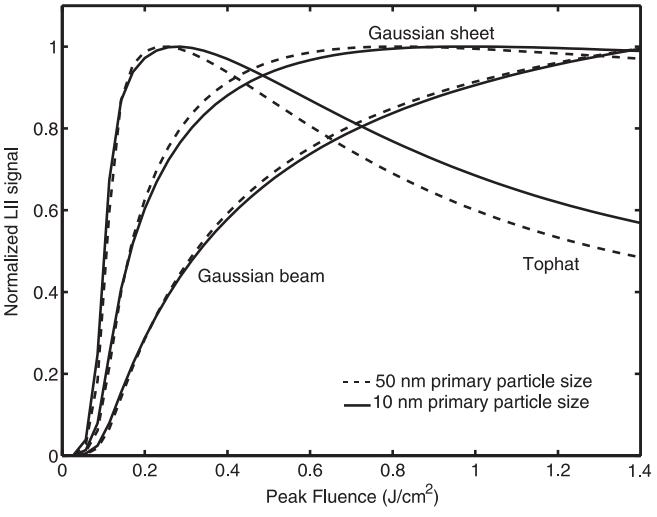

FIGURE 8 Modeled peak fluence curves from 100-ns gate starting before the laser pulse (zero delay). The curves corresponding to the Gaussian sheet show a plateau region as often found experimentally

We have chosen to plot the curves versus peak fluence since then all three cases have the same peak fluence vaporization threshold, here defined as the laser fluence at which vaporization starts somewhere in the measurement volume. Also, the temporal distribution of laser energy has to be considered for precise definition of the gate-delay time. In experiments the delay time is often defined from the start of the laser pulse. However, the temporal distribution of laser energy was in the present study modeled as Gaussian. Therefore, no obvious definition exists for defining the start of the pulse. We defined the delay as zero when the laser pulse has reached 1% of its maximum irradiance.

In Fig. 8 normalized fluence curves are shown for the three spatial energy distributions. The TIRE-LII signal has been integrated starting with a zero delay and going on for 100 ns. The vaporization threshold peak fluence for the calculations in Fig. 8 was shown to be $\sim 0.1\,\mathrm{J/cm^2}$. The calculations have been performed for two primary particle sizes with monodisperse distributions. Obviously the top-hat spatial energy distribution reaches a maximum and then decreases. The Gaussian sheet does in fact reach a plateau, while the Gaussian beam, though it levels out a bit, increases in the entire interval. The size of soot particles does not seem to have a great impact on the curves, but obviously the influence of this parameter differs for the energy distributions. The top-hat distribution seems to be most affected, while the Gaussian beam shows curves with high similarity.

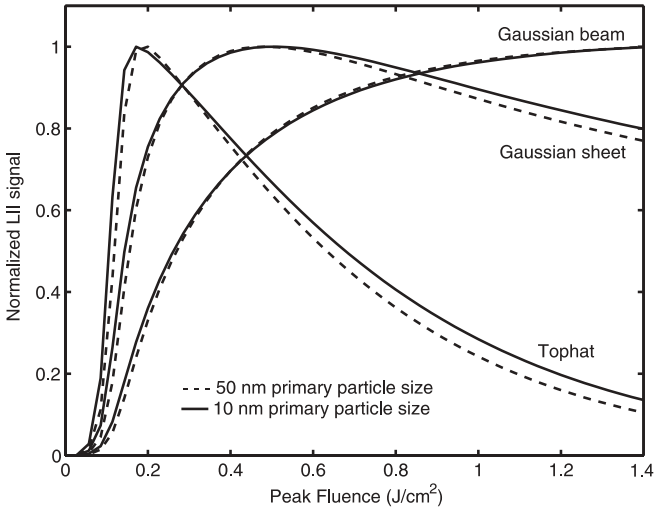

FIGURE 9 Fluence curves from 18-ns gate starting 20 ns after the start of the laser pulse. As the prompt signal is not integrated the impact of vaporization is larger on the curves

The choice of gate timing (integration interval) has a large impact on the fluence dependence of the integrated signal. With the integration interval of Fig. 8 both the prompt signal and parts of the decay are collected. Following Snelling et al. [18] the integration interval was set to start after the laser pulse (20-ns delay) and with just an 18-ns gate. The results here look quite different as depicted in Fig. 9. Here the vaporization process influences the signal to a higher extent than it did for the 100-ns integration presented in Fig. 8. This is because the prompt signal is not detected using this delayed gate. Tests with the model suggest that the prompt signal will have a rather small increase for increasing fluence, while the delayed signal drastically decreases because of the vaporization shrinking the particles as depicted in Fig. 7.

The use of a short delayed gate as in Fig. 9 may lead to poor signal to noise ratio – something that could be circumvented using a longer gate. The model predicts the signal to noise ratio to be improved by more than a factor of two by using a 100-ns gate instead of the 18-ns gate with the same delay time in both cases. However, the overall appearance of the normalized fluence curves does not differ, something that could be attributed to the fact that the heat transfer is by far the dominant process in the delayed time domain.

Obviously, the choice of gate timing affects the signal substantially. In Fig. 10 fluence curves for the 18-ns gate used for Fig. 9 have been presented for different choices of delay time. All curves are derived for a top-hat distribution of laser energy and the primary particle size was 10 nm. The large change in overall appearance of the curves is evident as the delay is in-

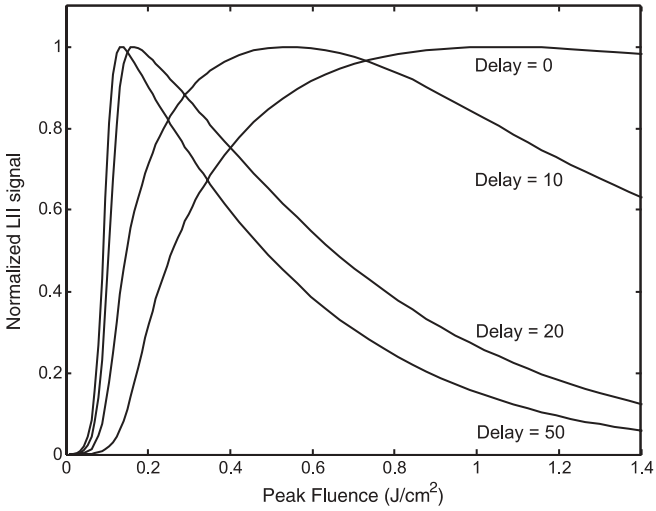

FIGURE 10 Fluence curves from 18-ns gate using different delay times. The curves are derived for the top-hat laser-energy distribution and the primary particle size is 10 nm

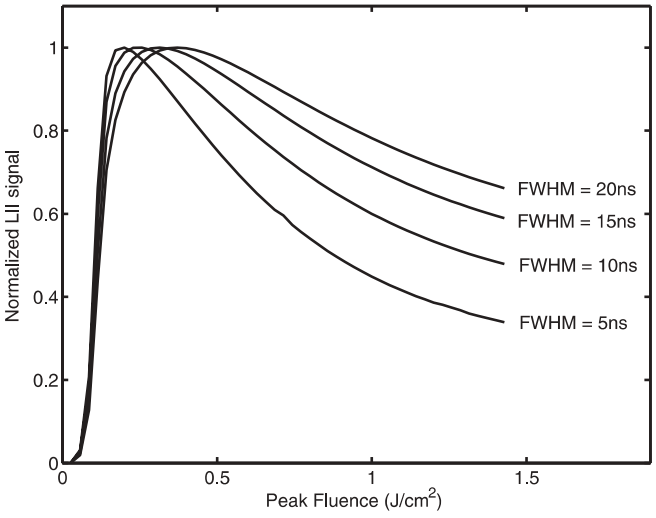

FIGURE 11 Fluence curves for a top-hat spatial energy distribution for different FWHMs of the temporal laser-energy distribution

creased. However, when the delay is long enough the shape only changes marginally.

6 Discussion

The overestimation of the particle size introduced when using a model assuming a monodisperse distribution was shown in Fig. 5. For none of the distributions tested did the bias get larger than 20% of the mean primary particle size. Compared to some other sources of error in the TIRE-LII model, some may argue that this error is of minor importance. Will et al. [10] have in a parameter study shown that uncertainty in the gas temperature is very critical. Their terms in the model are essentially the same as the ones used in this study, and comparisons are therefore possible. According to Will et al. uncertainties in absolute gas temperature must be at least 100 K for the relative error in evaluated primary particle size to approach 20%. For systems with totally unknown temperature the errors may be large but, using the Coherent Antistokes Raman Spectroscopy (CARS) technique, flame temperatures can be determined with uncertainties in the range of 50 K [26]. Thus, if the temperature is established, the influence of the bias due to the erroneous assumption of monodisperse particle distributions is even more important.

The fluence curves derived for different spatial laser-energy distributions show its importance for the overall signal. The model predicts a plateau region for the Gaussian sheet, which is a well-known experimental feature. The primary particle size does not seem to have a great impact on the curves, but the smaller particles do seem to reach the plateau regime for somewhat smaller fluences than do the larger particles.

It is of utmost importance to point out that the laser fluence really is not enough to fully describe the influence of the laser pulse on the LII signal. Since the fluence is not time dependent it does not take into account the temporal distribution of the laser pulse. In Fig. 11 the top-hat fluence curve for the 50-nm particles of Fig. 8 has been plotted for different FWHMs of the Gaussian temporal laser-energy distribution. The figure clearly shows the significance of taking the temporal distribution into account. During experiments with a specific laser system, the temporal distribution may be regarded as constant, and in that case the fluence can be used, but when comparing fluence curves measured using different lasers it is important to keep the influence of the temporal distribution in mind.

The influence of the spatial distribution of laser energy on the evaluated primary particle size is another very important issue. Since mass loss of the particles is modeled as surface vaporization, the primary particle size is altered by the laser, meaning that the decay constant may differ substantially for different laser-pulse energies. For non-uniform spatial laser-energy distributions with energies high enough for vaporization to occur, the particles in the measurement volume will be exposed to different energies, thus creating a rather large range of primary particle sizes. If vaporization is not taken into account, the evaluated primary particle size will here be biased towards smaller diameters. Experiments can be performed with low laser energies, thus avoiding vaporization altogether [11].

There are many uncertainties related to the model used in this study. Vander Wal et al. have in detailed investigations using TEM showed that the soot particles drastically change in structure after being exposed to a high-energy laser pulse [27, 28]. The shape, density and optical properties are likely to change because of this. This would surely affect the model predictions for higher fluences. Another important issue is the influence of the morphology on the evaluated primary particle size. If the structure makes the total surface area smaller than it would have been if the particles were not connected, the cooling rate would decrease, and the primary particle size would be overestimated. For structures where the primary particles are loosely connected in widespread structures the heat-transfer properties may be only marginally affected by the aggregate structure because the total area may be considered nearly the same as if the particles were not connected. In recent studies by Dankers et al., the aggregate structure showed no influence on the LII signals [29]. There is also the need for further development of the physical model for vaporization and heat conduction. There is

also some confusion regarding the choice of heat-transfer treatment in the model. There exist a number of expressions and it is not obvious which one is the best description for LII.

Because of the issues discussed above, we intend to pursue further investigations of the behavior of the extended theoretical model for TIRE-LII in the near future. The work so far has mainly been aimed at invoking the size distribution and the laser spatial energy distribution into the model. However, more detailed investigations of the parameters and terms in the heat- and mass-balance equations are intended as a second stage. In addition, specially designed experimental studies are planned in order to get a comparison with model predictions.

7 Conclusions

The temporal profile of a laser-induced incandescence signal is often used for evaluation of primary particle sizes in combustion systems. In this work a theoretical model for time-resolved laser-induced incandescence has been extended to include particle-size distributions and different spatial distributions of the laser energy.

When evaluating primary particle size, a monodisperse size distribution is often assumed, although it is well known that a polydisperse distribution is a better description of the real situation. The overestimation of the primary particle size because of this assumption has been quantified for Gaussian and lognormal size distributions of different widths. As an example, it was shown that the overestimation for a Gaussian distribution with a FWHM of 60% and an average primary particle size of 50 nm (that may be found in a real situation) gave an evaluated monodisperse primary particle size that was 18% higher than the average size for the distribution. Thus, the effect should not be neglected.

The dependence of the LII signal on the laser fluence is often used by experimentalists to find an appropriate laser-pulse energy to use during experiments. This so-called fluence curve was studied for different spatial distributions of the laser energy. It was established that the fluence curve was strongly dependent on whether the distribution was a top hat, Gaussian sheet or Gaussian beam. However, the influence on the fluence curve for different particle sizes was minor. Additional tests showed the behavior of the fluence curve for a change in gate width and position as well as for the time duration of the laser pulse.

In the near future, further theoretical work will be done in the development of the model, and experiments will be designed to test the modeling results.

ACKNOWLEDGEMENTS The financial support from the Swedish Research Council is gratefully acknowledged.

REFERENCES

1 T.R. Barfknecht: Prog. Energy Combust. Sci. **9**, 199 (1983)
2 L.A. Melton: Appl. Opt. **23**, 2201 (1984)
3 R.J. Santoro, C.R. Shaddix: in *Applied Combustion Diagnostics*, ed. by K. Kohse-Köinghaus, J.B. Jeffries (Taylor & Francis, London 2002) pp. 252–286
4 P.-E. Bengtsson, M. Aldén: Appl. Phys. B **60**, 51 (1995)
5 B. Axelsson, R. Collin, P.-E. Bengtsson: Appl. Phys. B **72**, 367 (2001)
6 R.L. Vander Wal: Proc. Combust. Inst. **27**, 59 (1998)
7 R.L. Vander Wal, T.M. Ticich: Appl. Opt. **38**, 1444 (1999)
8 C.J. Dasch: Appl. Opt. **23**, 2209 (1984)
9 D.L. Hofeldt: SAE paper 930079 (Society of Automotive Engineers, Warrendale, PA 1993)
10 S. Will, S. Schraml, K. Bader, A. Leipertz: Appl. Opt. **37**, 5647 (1998)
11 P. Roth, A.V. Filippov: J. Aerosol Sci. **27**, 95 (1996)
12 R.L. Vander Wal, T.M. Ticich, A.B. Stephens: Combust. Flame **116**, 291 (1999)
13 G.J. Smallwood, D.R. Snelling, F. Liu, Ö.L. Gülder: J. Heat Transfer **123**, 814 (2001)
14 B.J. McCoy, C.Y. Cha: Chem. Eng. Sci. **29**, 381 (1974)
15 A.V. Filippov, D.E. Rosner: Int. J. Heat Mass Transfer **43**, 127 (2000)
16 H.A. Michelsen: J. Chem. Phys. **118**, 7012 (2003)
17 P.O. Witze, S. Hochgreb, D. Kayes, H.A. Michelsen, C.R. Shaddix: Appl. Opt. **40**, 2443 (2001)
18 D.R. Snelling, F. Liu, G.J. Smallwood, Ö.L. Gülder: in *34th Natl. Heat Transfer Conf., NHTC2000-12132, 2000*, p. 1–9
19 W.H. Dalzell, A.F. Sarofim: J. Heat Transfer **91**, 100 (1969)
20 H.R. Leider, O.H. Krikorian, D.A. Young: Carbon **11**, 555, 1973
21 H. Bockhorn, F. Fetting, A. Heddrich: in *21st Int. Symp. Combustion* (The Combustion Institute, Pittsburgh, PA 1986) pp. 1001–1012
22 Ü.Ö. Köylü, G.M. Faeth: Combust. Flame **89**, 140 (1992)
23 B.L. Wersborg, J.B. Howard, G.C. Williams: in *14th Int. Symp. Combustion* (The Combustion Institute, Pittsburgh, PA 1973) pp. 929–940
24 T. Ni, J.A. Pinson, S. Gupta, R.J. Santoro: Appl. Opt. **34**, 7083 (1995)
25 N.P. Tait, D.A. Greenhalgh: Ber. Bunsenges. Phys. Chem. **97**, 1619 (1993)
26 A. Thumann, M. Schenk, J. Jonuscheit, T. Seeger, A. Leipertz: Appl. Opt. **36**, 3500 (1997)
27 R.L. Vander Wal, T.M. Ticich, A.B. Stephens: Appl. Phys. B **67**, 115 (1998)
28 R.L. Vander Wal, M.Y. Choi: Carbon **37**, 231 (1999)
29 S. Dankers, S. Schraml, S. Will, A. Leipertz: Chem. Eng. Technol. **25**, 1160 (2002)